Switchable and Tunable Terahertz Metamaterial Based on Vanadium Dioxide and Photosensitive Silicon

Xin Zhang , Guan Wang , Jia Liu , Shiyi Zuo , Meichen Li , Shuang Yang , Yang Jia , Yachen Gao *

Posted Date: 27 June 2023

doi: 10.20944/preprints202306.1936.v1

Keywords: Switchable; Tunable; THz; Electromagnetically induced transparency; Absorber

Article

Switchable and tunable terahertz metamaterial based on vanadium dioxide and photosensitive silicon

Xin Zhang [1], Guan Wang [1], Jia Liu [1], Shiyi Zuo [1], Meichen Li [1], Shuang Yang [1], Yang Jia [1,2] and Yachen Gao [1,*]

[1] Electronic Engineering College, Heilongjiang University, Harbin, 150080, China; hi400304@163.com (X.Z.); wang2687220886@163.com (G.W.); liu_jia1220@163.com (J.L.); 18846092825@163.com (S.Z.); lmchen_qwe@163.com (M.L.); slby2025@163.com (S.Y.)

[2] College of Communication and Electronic Engineering, Qiqihar University, Qiqihar 161000, China; jiayang_1990@163.com (Y.J.)

* Correspondence: gaoyachen@hlju.edu.cn

Abstract: A switchable and tunable terahertz (THz) metamaterial based on photosensitive silicon and Vanadium dioxide (VO_2) was proposed. By using finite-difference time-domain (FDTD) method, the transmission and reflective properties of the metamaterial were investigated theoretically. The results imply that, the metamaterial can realize a dual electromagnetically induced transparency (EIT) or two narrow-band absorption depending on the temperature of the VO_2. Additionally, the magnitude of the EIT and two narrow-band absorption can be tuned by varying the conductivity of photosensitive silicon (PSi) via pumping light. Correspondingly, the slow light effect accompanying the EIT can also be adjusted.

Keywords: Switchable; Tunable; THz; Electromagnetically induced transparency; Absorber

1. Introduction

Terahertz waves are electromagnetic waves with frequencies in the range of 0.1 THz to 10 THz and wavelengths in the range of 0.03 to 3 mm, between microwave and infrared. It has high potential for applications in sensing, communication, and imaging [1-3]. However, its development has been hampered by the limitations of natural materials. In recent years, with the advanced development of micro and nano processing technology [4-6], metamaterials with complex structures and increasingly small dimensions are also contributing to the rapid development of THz technology. Based on metamaterials, researchers have designed various efficient optical micro-nano devices such as absorbers [7-9], polarization converters [10,11], and EIT devices [12,13]. The EIT effect results from its high transmission peaks in the low-transmission region. Near the peak frequency large dispersion and group delays occur. The effect has very promising applications in the field of slow light and promotes the enhancement of optical non-linear effects and has an equally positive effect on the development of all-optical information devices such as optical caches, optical switches, and optical routers [14-17]. The absorption effect in terahertz metamaterials has promising applications in areas such as filters, stealth devices, and highly sensitive sensors [9,18]. However, conventional THz metamaterials cannot change their properties after they are fabricated and have a single function, which leads to high practical costs, which means tunable and switchable multifunctional terahertz metamaterials is necessary.

At present, the tuning of THz metamaterials is mainly based on active materials such as VO_2 and PSi, etc [19]. VO_2 is a transition metal oxide having the property of reversible phase transition. The phase transition temperature is about 340 K, which makes phase transition of VO_2 easy to control [19-22]. PSi is a semiconductor whose conductivity can be changed easily by tuning the intensity of light on it [23]. In 2012, J. Gu et al. combined

Preprints (www.preprints.org) | NOT PEER-REVIEWED | Posted: 27 June 2023 doi:10.20944/preprints202306.1936.v1

photoconductive silicon substrates with planar metamaterial units to achieve a THz EIT effect with photocontrolled configurability [24]. In 2016, Zhang et al. proposed dynamically modulated THz absorber combining VO_2 films with arrays of structured copper rings. The absorber achieved a modulation depth of approximately 78% under light induction [25]. In 2018, Liu et al. introduced a dynamically tunable THz metamaterial consisting of graphene and two cut-line metal resonance rings. They realized an EIT effect with an 81% modulation depth and an actively controlled slow light effect [26]. In 2020, Zheng et al. designed a tunable EIT terahertz metamaterial consisting of two Au split-disk resonant rings on top and bottom, with a modulation depth of 75.58% [27]. As can be seen, the studies above concerning THz metamaterials focused mainly on single function, and have lower modulation depth. In fact, it is necessary to develop new THz metamaterials having tunable multifunction and high modulation depth.

In this paper, we design a switchable THz metamaterial with tunable EIT effect and absorption based on PSi and VO_2. The metamaterial consists of a metal bar and two square resonant rings of different sizes forming a metal layer, a dielectric layer and a VO_2 film. The properties of the designed metamaterial are investigated theoretically by means of the FDTD method. It is found that, when the temperature of VO_2 is set to be room temperature it is in the dielectric state, and the metamaterial exhibits a double EIT effect and can achieve a double slow light effect. When the temperatures are above the phase transition temperature VO_2 is in a metal state, the metamaterial shows a double narrow-band absorption. When the conductivity of the PSi changes, the magnitude of EIT and absorption can be changed and both have a high modulation depth.

2. Materials and Methods

The designed metamaterial is arranged in a periodic pattern unit with P = 200 μm. As shown in Figure 1(a), from top to bottom, the unit consists of four layers which are metal layer, dielectric layer, VO_2 film, and dielectric layer. Correspondingly, the thickness of each layer is $h_1 = 3$ μm, $h_2 = 25$ μm, $h_3 = 0.2$ μm, and $h_4 = 14.8$ μm respectively. As shown in Figure 1(b), the metal layer consists of metal bar (MB), large resonant ring (LRR), small resonant ring (SRR). The length of MB is L = 160μm, and both SRR and LRR are square rings with side lengths of a = 30 μm and b = 35 μm respectively. The width of MB and ring is k = 5 μm. Each ring has a gap filled with 5 μm PSi. The distribution of each structure is given by $S_1 = 47.5$ μm, $S_2 = 5$ μm, $S_3 = 37.5$ μm.

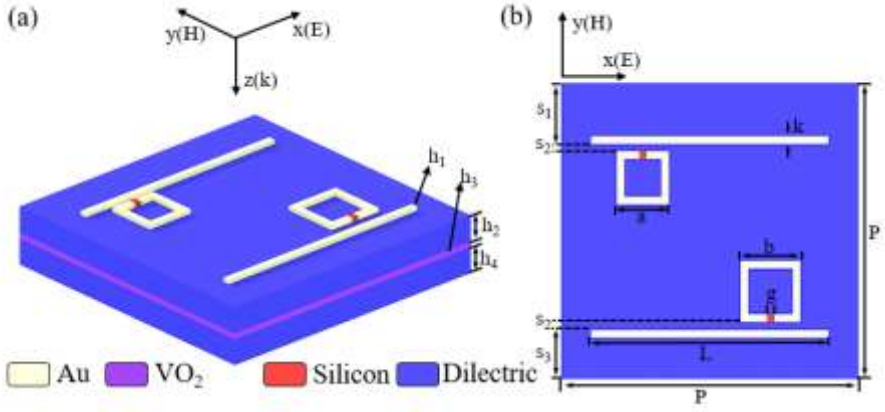

Figure 1. (a) Unit structure diagram, (b) Top view of unit structure.

The properties of the metamaterial were investigated using FDTD. When conducting simulation, the THz plane wave propagates in the Z-axis direction and its polarization is in the X-axis direction. In THz band, gold is considered to be a lossy metal, and its conductivity can be obtained to be 4.56×10^7 S/m via a static model [8]. The relative dielectric constants of dielectric and PSi are 2.9 and 11.9 respectively [28].

The optical properties of VO_2 are illustrated using the Drude model [29-33]:

Preprints (www.preprints.org) | NOT PEER-REVIEWED | Posted: 27 June 2023 doi:10.20944/preprints202306.1936.v1

$$\varepsilon(\omega) = \varepsilon_\infty - \frac{\omega_p^2(\sigma)}{\omega^2 + i\gamma\omega} \quad (1)$$

where $\varepsilon_\infty = 12$ is the dielectric constant of insulation at infinite frequency, and $\gamma = 5.75 \times 10^{13}$ rad/s is collision frequency. The plasma frequency can be characterized as $\omega_p^2(\sigma) = \omega_p^2(\sigma_0)\sigma/\sigma_0$, where $\omega_p(\sigma_0) = 1.4 \times 10^{15}$ rad/s, $\sigma_0 = 3 \times 10^5$ S/m. The conductivity of VO_2 is 1 S/m or 2×10^5 S/m when it is insulating or metal phase.

The conductivity of the PSi can be controlled by light and expressed as[34]:

$$\sigma_{si} = 4.863 \times 10^{-4} \times I^2 + 0.1856 \times I + 1.569 \quad (2)$$

where I is the intensity of the pump light. The conductivity of the PSi is 1 S/m and 1 x 10^5 S/m when the intensity of the pump light is 0 or 249 μJ/cm², respectively [23]. VO_2 can also be excited by pump light, but its excitation intensity is 8 mJ/cm², which is much greater than the excitation intensity of PSi [35], so the excitation of pump light to PSi has almost no effect on VO_2.

3. Results and discussion

3.1. Electromagnetically induced transparency

Firstly, we studied theoretically the transmission properties of the metamaterial when VO_2 is below the phase change temperature and the pumping light of the PSi is off. In the case, the conductivity of VO_2 and PSi is 1 S/m, and the results are shown in Figure 2(a). We can see that, there are two transmission peaks at 0.73 THz and 0.862 THz, defined as PEAK 1 and PEAK 2 respectively. In order to investigate the origin of the transmission peaks, we individually calculated the transmissions of the MB array, the SRR array, and the LRR array which are shown in Figure 2(b) using black, red and blue solid lines. Specifically, MB array shows a broadband valley around the frequency of 0.723 THz, which is usually believed to result from Lorentzian resonance caused by incident light [28]. However, the SRR and LRR arrays produce two ultra-narrow transmission valleys at 0.909 THz and 0.778 THz respectively, which is usually believed to result from LC Resonance caused by incident light [24]. The transmittance peaks1,2 arise from the coupling of the narrowband mode and broadband modes, in which the broadband mode is referred to as bright mode and the narrowband mode as dark mode [36]. The bright and dark modes produce destructive interference at specific frequencies due to their different bandwidths, leading to the EIT effect [13].

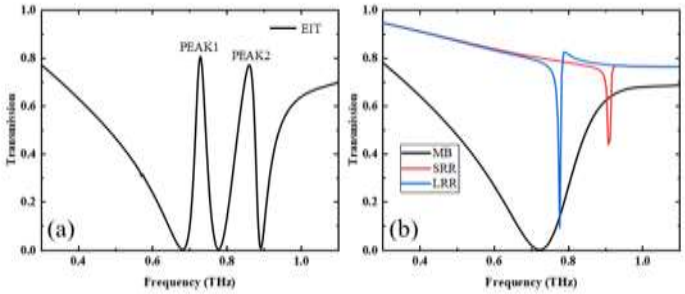

Figure 2. (a) Transmission spectra of structures consisting of MBs, SRRs and LRRs at a conductivity of 1S/m for both PSi and VO_2, SRR, LRR, (b) Transmission spectra of individual structures of MB.

To further explain the formation of the two EIT transmission peaks, as shown in Figure 3(a, b), we provided the electric field distribution at 0.73 THz and 0.862 THz, respectively. The EIT effect transmission PEAK 1 at 0.73 THz generates from the coupling of the LRR and the MB, while the EIT transmission PEAK 2 at 0.862 THz results from the coupling of the SRR ring and the MB [28]. The two different coupling produce two EIT transmission peaks in the transmission spectrum, achieving a double channel effect.

Preprints (www.preprints.org) | NOT PEER-REVIEWED | Posted: 27 June 2023 doi:10.20944/preprints202306.1936.v1

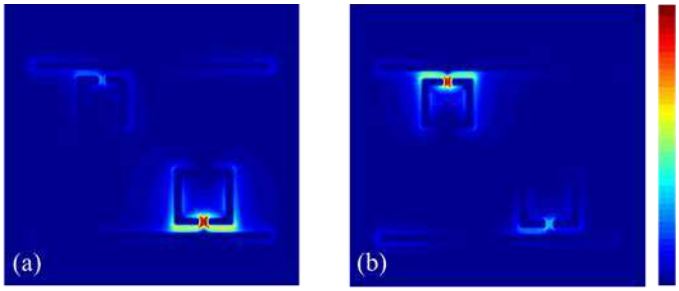

Figure 3. Electric field diagram of the EIT transmission peak at (a) 0.73 THz (b) 0.862 THz.

Secondly, we studied the transmission properties and slow light effect of the metamaterial when the temperature of VO_2 is below the phase change temperature and the pumping light of the PSi is on. In the case, the conductivity of VO_2 is still 1 S/m, the conductivity of PSi increase from 1 S/m to 240 S/m. The transmission characteristics of the metamaterial are shown in Figure 4(a), where we can see that, the peak transmittance at 0.73 THz and 0.862 THz are 0.804 and 0.769 respectively at 1 S/m for PSi. As the conductivity of the PSi increases, the amplitude of peaks 1, 2 begins to decrease and the peak frequency at PEAK 2 begins to red-shift. When the conductivity of the PSi reaches 240 S/m, the peak transmittance at frequencies of 0.73 THz and 0.862 THz are 0.08 and 0.31 respectively, and the transmittance spectral curve becomes an approximate Lorentz curve. The decrease of the transmission is due to the modulation of the dark mode by the increased conductivity of PSi. The PSi is located at the SRR and LRR notch, and an increase in its conductivity causes a decrease of the resonant strength of the SRR and LRR, affecting the coupling of the SRR and LRR with the CW, which in turn affects the amplitude and frequency position of peaks 1, 2 [24]. The modulation depth of the transmission peak can be expressed as [13]:

$$\frac{\Delta T}{T_0} = \frac{|T_0 - T_1|}{T_0} \tag{3}$$

where T_0 and T_1 are the transmittance of the PSi conductivity at 1 S/m and 240 S/m respectively. Where T_0 and T_1 at 0.73 THz were 0.804 and 0.08 respectively, and T_0 and T_1 at 0.862 THz were 0.769 and 0.31 respectively. Using equation (3) we can solve for a modulation depth of 90.05% and 59.69% at 0.73 THz and 0.862 THz respectively.

The slow light effect is an important application of EIT and is often described by the group delay：

$$G = \frac{d\varphi}{d\omega} \tag{4}$$

where φ is the phase shift of EIT and $\omega = 2\pi f$ is the angular frequency of EIT [13]. Figures 4(b) and 4(c) show the phase shift and group delay of the EIT effect for different conductivities of PSi in Figure 4(a). When the conductivity of PSi is 1 S/m, the phase shift shows steep jumps near the two transmission peaks and achieves group delays of 8.79 ps and 9.04 ps. As the conductivity increases, the phase shift decreases, and group delay gradually diminishes. When the conductivity of the PSi reaches 240 S/m, the phase shift jumps and group delay properties almost disappear, and the slow light effect caused by the MB gradually becomes apparent. Thus, the regulation of the double slow light effect can be achieved by changing the conductivity of the PSi.

Preprints (www.preprints.org) | NOT PEER-REVIEWED | Posted: 27 June 2023 doi:10.20944/preprints202306.1936.v1

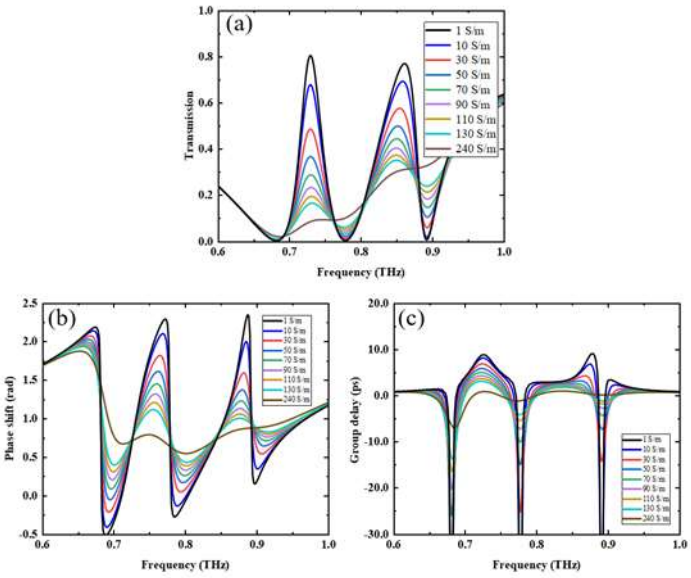

Figure 4. (a) transmission spectrum, (b) phase shift spectrum, (c) group delay variation of PSi at different conductivities for a VO_2 conductivity of 1 S/m.

3.2. Absorption

When the pumping power of the PSi is off, its conductivity is 1 S/m. When VO_2 is above the phase change temperature, its conductivity is 2×10^5 S/m, it is in metal state. In the case, we studied the absorption properties of the metamaterial. Absorbance can be calculated using A = 1-R-T=1-$|S_{11}|^2$-$|S_{21}|^2$, where R stands for reflectance and T for transmittance, and the S_{11} and S_{21} are the reflection and transmission coefficients obtained from the S-parameters [37]. The thickness of VO_2 film is 200 nm, and larger than the terahertz crust depth, which makes terahertz almost impermeable [9], so T=0, A=1-R=1-$|S_{11}|^2$. The reflection spectrum was calculated using FDTD, correspondingly the absorption spectrum was obtained and shown in Figure 5(a) where two absorption peaks are at 0.752 THz and 0.885 THz, respectively.

We studied the origin of the absorption peaks using impedance matching theory shown as follows [38-40]:

$$A = 1 - R = 1 - \left|\frac{Z - Z_0}{Z + Z_0}\right|^2 = 1 - \left|\frac{Z_r - 1}{Z_r + 1}\right|^2 \quad (5)$$

$$Z_r = \pm\sqrt{\frac{(1 + S_{11})^2 - {S_{21}}^2}{(1 - S_{11})^2 - {S_{21}}^2}} \quad (6)$$

Where Z is the effective impedance, Z_0 is the free space impedance, the relative impedance expressed as $Z_r = Z/Z_0$. When $Z_r = 1$ the absorption rate is 1 and the impedance of the metamaterial matches that of free space. Figure 5 (b) shows the corresponding impedance plots, where the real part and imaginary part of the relative impedance Z_r are shown with black and red lines respectively. At p_1 and p_2, the real and imaginary values of the relative impedance Z_r are 1 and 0, respectively, which means impedance matching occurs here. The same effect happens at p_3 and p_4, p_1, p_2 and p_3, and p_4 present evidence of perfect absorption at 0.752 THz and 0.885 THz, respectively.

Preprints (www.preprints.org) | NOT PEER-REVIEWED | Posted: 27 June 2023 doi:10.20944/preprints202306.1936.v1

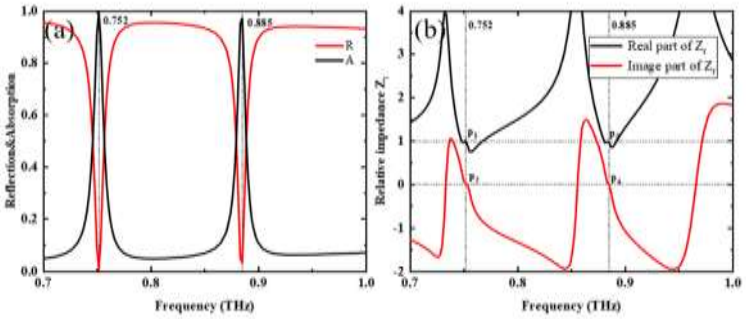

Figure 5. (a) Absorption spectra of metamaterials with PSi conductivity of 1 S/m and VO_2 conductivity of 2×10^5 S/m, (b) Schematic diagram of the real and imaginary parts of impedance matching.

To further explain the formation of the two absorption peaks, we calculated the electric field distribution of the structure at frequencies of 0.752 THz and 0.885 THz which were shown in Figures 6(a) and (b), respectively. From Figure 6(a), we can find that the electric field enhancement is mainly distributed in the gap between the LRR and the MB, which means the absorption peak at 0.752 THz mainly originates from the coupling of the LRR to the MB. From Figure 6(b), we can find that the electric field enhancement is mainly distributed in the gap between the SRR and the MB, which means the absorption peak at 0.885 THz mainly originates from the coupling of the SRR to the MB. The two different coupling modes produce a double narrow-band absorption peak in the absorption spectrum.

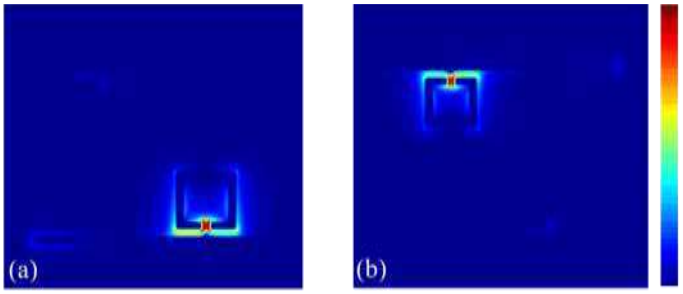

Figure 6. Electric field diagram of the absorption peak at (a) 0.752 THz (b) 0.885 THz.

In addition, we studied the absorption properties of the metamaterial when VO_2 is above the phase change temperature and the pumping power of the PSi is on. In the case, the conductivity of VO_2 is 2×10^5 S/m and the conductivity of PSi is adjusted from 1 S/m to 10^5 S/m by changing the intensities of pump light. Figure 7 shows the change of absorption with the conductivity of PSi. When the conductivity is 1 S/m, absorption peak is the highest. As the conductivity increases, absorption peak decrease gradually. When the conductivity is 10^5 S/m, absorption peak disappears, which means that the resonance between LRR and SRR and MB disappears.

In fact, at peak frequency, the conductivity of the PSi located at the SRR and LRR notches affects the impedance match between the metamaterial and the free space. High conductivity causes weak match and low absorption [9]. Specifically, when the conductivity of PSi is 1 S/m or 10^5 S/m, the amplitude of absorption at 0.752 THz and 0.885 THz were 0.998, 0.97 or 0.036, 0.055, respectively. So the modulation depths of the structure can be obtained via equation (3) to be 96.39% and 94.33% at 0.752 THz and 0.885 THz frequencies respectively.

Preprints (www.preprints.org) | NOT PEER-REVIEWED | Posted: 27 June 2023 doi:10.20944/preprints202306.1936.v1

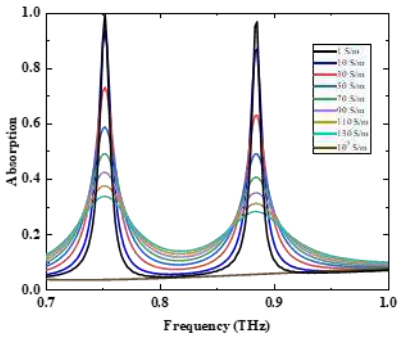

Figure 7. Absorption spectra of PSi at different conductivities when the conductivity of VO_2 is 2×10^5 S/m

For comparison, in Table 1 we list some work concerning. From the table, we found that the proposed structure has higher modulation depth of EIT effect. Moreover, it also has higher absorption modulation depth.

Table 1. Comparison of designed metamaterials with reported metamaterials.

Reference	Adjustable Material	Maximum modulation depth through the peak (EIT)	Maximum modulation depth of peak absorption
[26]	graphene	81%	none
[27]	none	75.58%	none
[41]	VO_2 & graphene	70%	90%
[25]	VO_2	none	78%
This work	Silicon & VO_2	90.05%	96.39%

4. Conclusions

In summary, we have designed a dual-function switchable and tunable THz metamaterial by using VO_2 and PSi. When VO_2 is in the dielectric state, the THz metamaterial produces a double EIT effect at frequencies of 0.73 THz and 0.862 THz and achieves group delays of 8.79 ps and 9.04 ps. And varying the conductivity of PSi can tune the amplitude of transmission peak and group delay. When VO_2 is in the metallic state, the metamaterial produced two perfect absorption peaks at 0.752 THz and 0.885 THz. And the amplitude of absorption peak could be tuned by varying the conductivity of PSi. The modulation depths of the two absorption peaks can reach 96.39% and 94.33% respectively. Compared to previous designs, we have achieved dual-function integration with higher modulation depths for each function, breaking the limitations of single-function and showing potential applications such as slow-light devices, filters and sensors.

Author Contributions: Conceptualization, X.Z. and Y.G.; methodology, X.Z. and Y.G.; software, X.Z. and Y.G.; validation, X.Z., G.W. and Y.G.; formal analysis, X.Z. and J.L.; investigation, X.Z., S.Z., M.L., S.Y., Y.J. and Y.G.; writing—original draft preparation, X.Z.; writing—review and editing, X.Z. and Y.G.; funding acquisition, Y.G. All authors have read and agreed to the published version of the manuscript.

Funding: Natural Science Foundation of Heilongjiang Province (LH2020F041). Fundamental Research Funds in Heilongjiang Provincial Universities (145209148).

Data Availability Statement: All content and data have been displayed in the manuscript.

Conflicts of Interest: The authors declare no conflict of interest.

References

1. Otter, W.J.; Lucyszyn, S. Hybrid 3-D-Printing Technology for Tunable THz Applications. *Proceedings of the Ieee* **2017**, *105*, 756-767, doi:10.1109/jproc.2016.2629958.
2. Wang, J.; Tian, H.; Wang, Y.; Li, X.Y.; Cao, Y.J.; Li, L.; Liu, J.L.; Zhou, Z.X. Liquid crystal terahertz modulator with plasmon-induced transparency metamaterial. *Optics Express* **2018**, *26*, 5769-5776, doi:10.1364/oe.26.005769.
3. Zhang, M.J.; Hong, H.C.; Lin, H.J.; Shen, L.G.; Yu, H.Y.; Ma, G.C.; Chen, J.R.; Liao, B.Q. Mechanistic insights into alginate fouling caused by calcium ions based on terahertz time-domain spectra analyses and DFT calculations. *Water Research* **2018**, *129*, 337-346, doi:10.1016/j.watres.2017.11.034.
4. Fang, N.; Lee, H.; Sun, C.; Zhang, X. Sub-diffraction-limited optical imaging with a silver superlens. *Science (New York, N.Y.)* **2005**, *308*, 534-537, doi:10.1126/science.1108759.
5. Schurig, D.; Mock, J.J.; Justice, B.J.; Cummer, S.A.; Pendry, J.B.; Starr, A.F.; Smith, D.R. Metamaterial electromagnetic cloak at microwave frequencies. *Science (New York, N.Y.)* **2006**, *314*, 977-980, doi:10.1126/science.1133628.
6. Zheludev, N.I. The Road Ahead for Metamaterials. *Science* **2010**, *328*, 582-583, doi:10.1126/science.1186756.
7. Barzegar-Parizi, S.; Ebrahimi, A. Ultrathin, polarization-insensitive multi-band absorbers based on graphene metasurface with THz sensing application. *Journal of the Optical Society of America B-Optical Physics* **2020**, *37*, 2372-2381, doi:10.1364/josab.396266.
8. Liu, W.W.; Song, Z.Y. Terahertz absorption modulator with largely tunable bandwidth and intensity. *Carbon* **2021**, *174*, 617-624, doi:10.1016/j.carbon.2020.12.001.
9. Wang, G.; Wu, T.; Jia, Y.; Gao, Y.; Gao, Y.C. Switchable Terahertz Absorber from Single Broadband to Dual Broadband Based on Graphene and Vanadium Dioxide. *Nanomaterials* **2022**, *12*, doi:10.3390/nano12132172.
10. Li, J.S.; Li, X.J. Switchable tri-function terahertz metasurface based on polarization vanadium dioxide and photosensitive silicon. *Optics Express* **2022**, *30*, 12823-12834, doi:10.1364/oe.454240.
11. Liao, S.Y.; Sui, J.Y.; Zhang, H.F. Switchable ultra-broadband absorption and polarization conversion metastructure controlled by light. *Optics Express* **2022**, *30*, 34172-34187, doi:10.1364/oe.472336.
12. Liu, N.; Langguth, L.; Weiss, T.; Kastel, J.; Fleischhauer, M.; Pfau, T.; Giessen, H. Plasmonic analogue of electromagnetically induced transparency at the Drude damping limit. *Nature Materials* **2009**, *8*, 758-762, doi:10.1038/nmat2495.
13. Wu, T.; Shao, Y.B.; Buyingaridi; Ma, S.; Gao, Y.C. Terahertz hybrid metal-graphene metamaterials with tunable dual-band electromagnetically induced transparency. *Optik* **2021**, *240*, doi:10.1016/j.ijleo.2021.166784.
14. Chen, H.; Zhang, H.Y.; Liu, M.D.; Zhao, Y.K.; Liu, S.D.; Zhang, Y.P. Tunable multiple plasmon-induced transparency in three-dimensional Dirac semimetal metamaterials. *Optics Communications* **2018**, *423*, 57-62, doi:10.1016/j.optcom.2018.04.021.
15. Jiang, Y.; Ning, H.Y.; Tian, C.G.; Jiang, B.J.; Li, Q.; Yan, H.J.; Zhang, X.L.; Wang, J.Q.; Jing, L.Q.; Fu, H.G. Single-crystal TiO2 nanorods assembly for efficient and stable cocatalyst-free photocatalytic hydrogen evolution. *Applied Catalysis B-Environmental* **2018**, *229*, 1-7, doi:10.1016/j.apcatb.2018.01.079.
16. Zhao, J.X.; Song, J.L.; Zhou, Y.; Zhao, R.L.; Zhou, J.H. Tunable multiple plasmon-induced transparency in a simple terahertz Dirac semimetal based metamaterial. *Optical Materials Express* **2019**, *9*, 3325-3332, doi:10.1364/ome.9.003325.
17. Wu, T.; Wang, G.; Jia, Y.; Shao, Y.B.; Gao, Y.; Gao, Y.C. Multi-control plasmon-induced transparency via graphene and bulk Dirac semimetal. *Diamond and Related Materials* **2022**, *129*, doi:10.1016/j.diamond.2022.109369.
18. Alves, F.; Kearney, B.; Grbovic, D.; Karunasiri, G. Narrowband terahertz emitters using metamaterial films. *Optics Express* **2012**, *20*, 21025-21032, doi:10.1364/oe.20.021025.
19. Jeong, Y.G.; Han, S.; Rhie, J.; Kyoung, J.S.; Choi, J.W.; Park, N.; Hong, S.; Kim, B.J.; Kim, H.T.; Kim, D.S. A Vanadium Dioxide Metamaterial Disengaged from Insulator-toMetal Transition. *Nano Letters* **2015**, *15*, 6318-6323, doi:10.1021/acs.nanolett.5b02361.
20. Dicken, M.J.; Aydin, K.; Pryce, I.M.; Sweatlock, L.A.; Boyd, E.M.; Walavalkar, S.; Ma, J.; Atwater, H.A. Frequency tunable near-infrared metamaterials based on VO_2 phase transition. *Optics Express* **2009**, *17*, 18330-18339, doi:10.1364/oe.17.018330.

21. Kats, M.A.; Sharma, D.; Lin, J.; Genevet, P.; Blanchard, R.; Yang, Z.; Qazilbash, M.M.; Basov, D.N.; Ramanathan, S.; Capasso, F. Ultra-thin perfect absorber employing a tunable phase change material. *Applied Physics Letters* **2012**, *101*, doi:10.1063/1.4767646.
22. Wen, Q.Y.; Zhang, H.W.; Yang, Q.H.; Xie, Y.S.; Chen, K.; Liu, Y.L. Terahertz metamaterials with VO_2 cut-wires for thermal tunability. *Applied Physics Letters* **2010**, *97*, doi:10.1063/1.3463466.
23. Shen, N.H.; Massaouti, M.; Gokkavas, M.; Manceau, J.M.; Ozbay, E.; Kafesaki, M.; Koschny, T.; Tzortzakis, S.; Soukoulis, C.M. Optically Implemented Broadband Blueshift Switch in the Terahertz Regime. *Physical Review Letters* **2011**, *106*, doi:10.1103/PhysRevLett.106.037403.
24. Gu, J.Q.; Singh, R.; Liu, X.J.; Zhang, X.Q.; Ma, Y.F.; Zhang, S.; Maier, S.A.; Tian, Z.; Azad, A.K.; Chen, H.T.; et al. Active control of electromagnetically induced transparency analogue in terahertz metamaterials. *Nature Communications* **2012**, *3*, doi:10.1038/ncomms2153.
25. Zhang, H.; Jiang, P.; Xu, X.F. Study on a terahertz modulator based on metamaterial with photoinduced vanadium dioxide film. *Journal of Modern Optics* **2016**, *63*, 1073-1077, doi:10.1080/09500340.2015.1125960.
26. Liu, C.X.; Liu, P.G.; Yang, C.; Lin, Y.; Zha, S. Dynamic electromagnetically induced transparency based on a metal-graphene hybrid metamaterial. *Optical Materials Express* **2018**, *8*, 1132-1142, doi:10.1364/ome.8.001132.
27. Zheng, D.Y.; Lin, Y.S. Tunable Dual-Split-Disk Resonator with Electromagnetically Induced Transparency Characteristic. *Advanced Materials Technologies* **2020**, *5*, doi:10.1002/admt.202000584.
28. Ren, K.; He, Y.M.; Ren, X.B.; Zhang, Y.; Han, Q.; Wang, L.D.; Xu, M.J. Dynamically tunable multi-channel and polarization-independent electromagnetically induced transparency in terahertz metasurfaces. *Journal of Physics D-Applied Physics* **2020**, *53*, doi:10.1088/1361-6463/ab60ed.
29. Song, Z.Y.; Deng, Y.D.; Zhou, Y.G.; Liu, Z.Y. Terahertz toroidal metamaterial with tunable properties. *Optics Express* **2019**, *27*, 5792-5797, doi:10.1364/oe.27.005792.
30. Ding, F.; Zhong, S.M.; Bozhevolnyi, S.I. Vanadium Dioxide Integrated Metasurfaces with Switchable Functionalities at Terahertz Frequencies. *Advanced Optical Materials* **2018**, *6*, doi:10.1002/adom.201701204.
31. Liu, M.K.; Hwang, H.Y.; Tao, H.; Strikwerda, A.C.; Fan, K.B.; Keiser, G.R.; Sternbach, A.J.; West, K.G.; Kittiwatanakul, S.; Lu, J.W.; et al. Terahertz-field-induced insulator-to-metal transition in vanadium dioxide metamaterial. *Nature* **2012**, *487*, 345-348, doi:10.1038/nature11231.
32. Wang, S.X.; Kang, L.; Werner, D.H. Hybrid Resonators and Highly Tunable Terahertz Metamaterials Enabled by Vanadium Dioxide (VO_2). *Scientific Reports* **2017**, *7*, doi:10.1038/s41598-017-04692-8.
33. Zhu, Y.H.; Zhao, Y.; Holtz, M.; Fan, Z.Y.; Bernussi, A.A. Effect of substrate orientation on terahertz optical transmission through VO_2 thin films and application to functional antireflection coatings. *Journal of the Optical Society of America B-Optical Physics* **2012**, *29*, 2373-2378, doi:10.1364/josab.29.002373.
34. Cheng, Y.Z.; Gong, R.Z.; Zhao, J.C. A photoexcited switchable perfect metamaterial absorber/reflector with polarization-independent and wide-angle for terahertz waves. *Optical Materials* **2016**, *62*, 28-33, doi:10.1016/j.optmat.2016.09.042.
35. Xu, J.; Tang, J.; Cheng, Y.; Chen, M.; Wang, H.X.; Xiong, J.F.; Wang, T.R.; Wang, S.Z.; Zhang, Y.D.; Wen, H.; et al. Multifunctional analysis and verification of lightning-type electromagnetic metasurfaces. *Optics Express* **2022**, *30*, 17008-17025, doi:10.1364/oe.458412.
36. Liu, T.T.; Wang, H.X.; Liu, Y.; Xiao, L.S.; Yi, Z.; Zhou, C.B.; Xiao, S.Y. Active manipulation of electromagnetically induced transparency in a terahertz hybrid metamaterial. *Optics Communications* **2018**, *426*, 629-634, doi:10.1016/j.optcom.2018.06.018.
37. Qiu, Y.; Yan, D.X.; Feng, Q.Y.; Li, X.J.; Zhang, L.; Qiu, G.H.; Li, J.N. Vanadium dioxide-assisted switchable multifunctional metamaterial structure. *Optics Express* **2022**, *30*, 26544-26556, doi:10.1364/oe.465062.

38. Smith, D.R.; Vier, D.C.; Koschny, T.; Soukoulis, C.M. Electromagnetic parameter retrieval from inhomogeneous metamaterials. *Physical review. E, Statistical, nonlinear, and soft matter physics* **2005**, *71*, 036617, doi:10.1103/PhysRevE.71.036609.
39. Zhao, Y.; Huang, Q.P.; Cai, H.L.; Lin, X.X.; Lu, Y.L. A broadband and switchable VO_2-based perfect absorber at the THz frequency. *Optics Communications* **2018**, *426*, 443-449, doi:10.1016/j.optcom.2018.05.085.
40. Costa, F.; Genovesi, S.; Monorchio, A.; Manara, G. A Circuit-Based Model for the Interpretation of Perfect Metamaterial Absorbers. *Ieee Transactions on Antennas and Propagation* **2013**, *61*, 1201-1209, doi:10.1109/tap.2012.2227923.
41. Li, H.; Xu, W.H.; Cui, Q.; Wang, Y.; Yu, J. Theoretical design of a reconfigurable broadband integrated metamaterial terahertz device. *Optics Express* **2020**, *28*, 40060-40074, doi:10.1364/oe.414961.